GaN Nucleation and Growth on Sapphire (0001): Incorporation and Interlayer Transport

A. R. Woll,[1] R. L. Headrick,[2] S. Kycia,[2] and J. D. Brock[1]
[1]*School of Applied and Engineering Physics, Cornell University, Ithaca, New York 14853*
[2]*Cornell High Energy Synchrotron Source, Cornell University, Ithaca, New York 14853*
(Received 17 June 1999)

GaN growth on nitridated sapphire (0001) by rf plasma-assisted metal-organic molecular-beam epitaxy is shown to exhibit a highly superlinear growth rate and a transition from strained, smooth growth to relaxed cluster growth during the first layer. A coupled rate-equation model suggests that the growth rate arises from both the site-dependent reactivity of precursor molecules and a layer-dependent interlayer transport probability. The nitridation layer, which determines the initial strain of the GaN film, bears a striking resemblance to a well known Al-rich surface reconstruction of sapphire.

PACS numbers: 68.55.–a, 61.10.–i, 81.05.Ea, 81.15.Hi

During the last several decades, many of the atomistic processes which occur on growing surfaces during epitaxy have been identified [1]. However, in many cases of technological importance, determining which of these processes controls the morphological and microstructural evolution of the growing film remains a considerable challenge. For example, epitaxy of $In_xGa_{1-x}As/GaAs$ and Si/Ge is complicated by the role of lattice-mismatch induced strain [2,3]. In addition, the presence of surface reconstructions can dramatically affect the orientation and structure of epitaxial thin films [4]. Further complexity arises from the fact that many new and established epitaxial growth processes employ gas-source chemical beam techniques. During gas-source growth, incorporation of a constituent atom requires both adsorption onto the surface and decomposition of the molecular precursor. This leads to phenomena, such as nonlinear growth, that are associated with the kinetics of molecular reaction, incorporation, and desorption [5,6].

In this Letter we demonstrate that substrate surface structure, thin film strain, and incorporation kinetics all play an important role in determining the growth mode and structure during GaN growth on sapphire (0001). In particular, we report real-time x-ray fluorescence, reflectivity, and scattering measurements of the initial stages of growth of a thin film of $(000\bar{1})$ GaN using RF plasma-assisted metal-organic molecular-beam epitaxy (MOMBE). The data exhibit the following features: (i) the growth rate is highly superlinear during the growth of the first few GaN bilayers (BLs); (ii) the growth changes from a two- to a three-dimensional mode near the completion of the first GaN BL; (iii) a stable reconstruction forms on the sapphire (0001) surface during nitridation; and (iv) while the first BL is pseudomorphic to this reconstruction, subsequent growth proceeds via the nucleation and growth of strain-relaxed GaN clusters. Quantitative comparison of the growth rate and reflectivity data to a coupled rate-equation model supports a description based purely on kinetic processes.

These measurements were performed at the Cornell High Energy Synchrotron Source (CHESS) using an ultra-high vacuum surface diffraction chamber described elsewhere [5,7]. X rays of 11.0 keV with a bandwidth of 100 eV were used to simultaneously perform elastic and inelastic scattering measurements. An energy resolving Si(Li) detector was used to measure the intensity of inelastic Ga Kα emission (9.2 keV) from Ga atoms incorporated into the film. This intensity is directly proportional to film thickness [8]. Elastically scattered x rays were separated from the Ga Kα emission by the (0002) Bragg reflection of a pyrolytic graphite crystal analyzer and counted by a NaI detector. Reflectivity data were collected at the disallowed GaN (0001) or "anti-Bragg" position in order to maximize sensitivity to surface roughness. Grazing angle x-ray diffraction data were taken with an incidence angle of 0.5°.

The sapphire (0001) substrates were degreased and etched in hot phosphoric acid before being introduced into the vacuum chamber. A plasma source generated ≈18 eV nitrogen ions from an N_2 flow of 5 sccm (200 μmol/min) used both for nitridating the sapphire substrate and for growing the GaN film. The flux of triethylgallium (TEG), the gallium precursor, was set by a mass flow controller to 0.5 sccm (20 μmol/min) for all the experiments described below, yielding a steady-state growth rate of ≈1.1 BL/s. Under these conditions, the growth rate is proportional to TEG flow [9]. After a 5 min anneal at 1000 °C, the substrate was exposed to the nitrogen ion beam for 10 min. The sample was then cooled to ≈700 °C. The ion shutter was reopened for 60 sec just prior to growth. Subsequently, growth was initiated using a run/vent system to direct TEG flow into the growth chamber with an equilibration time of less than a second.

Figure 1a shows the intensity of the Ga Kα fluorescence x rays as a function of time for a typical growth run. The growth rate is highly nonlinear, increasing by approximately 2 orders of magnitude from $t = 0$ to $t = 20$ sec. The inset is a blowup of the growth rate during the first 10 sec and emphasizes this change in slope. Figure 1b shows the behavior of the specular reflectivity observed simultaneously with the fluorescence shown in Fig. 1a. Initially, the intensity begins to oscillate in a manner similar to

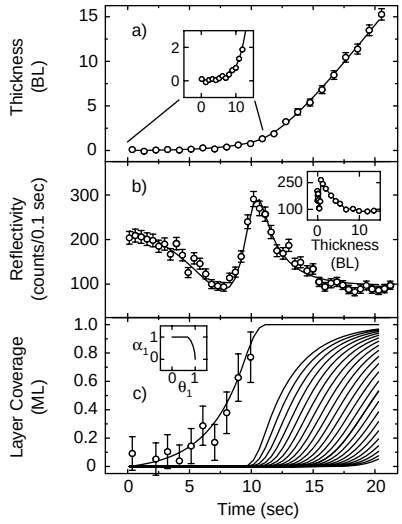

FIG. 1. (a) *In situ* Ga Kα fluorescence measurements of film thickness. The inset shows the early time behavior. (b) X-ray reflectivity at the GaN (0001) position during growth. The inset shows the same data plotted versus film thickness. The solid lines in (a) and (b) are calculated from the layer occupancies shown in (c). (c) Time dependence of the individual layer occupancies from the coupled rate-equation growth model resulting from a fit to the data in (a) and (b). The inset shows the behavior of α_1, the probability for atoms to transport from the second layer down to the first. The data from (a) are replotted to show that the initial nonlinearity in growth rate is determined by the behavior of the first layer.

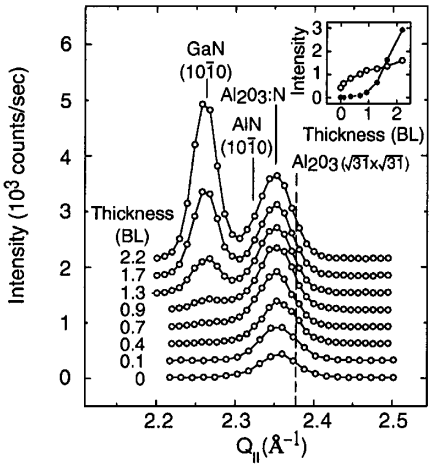

FIG. 2. Grazing incidence radial scans taken at several GaN film thicknesses near the GaN $(1, 0, \bar{1}, 0.1)$. The solid lines are guides to the eye. Peaks are observed at $Q_{\|} = 2.26$ and 2.35 Å^{-1}, corresponding to the positions of relaxed GaN $(10\bar{1}0)$ and α-$Al_2O_3(0001)$:N, respectively. For reference, the dashed line at $Q_{\|} = 2.378$ Å^{-1} indicates the radial position of the α-$Al_2O_3(0001)$ $(\sqrt{31} \times \sqrt{31})R \pm 9°$ $(6, 4)$ reflection [11]. The inset shows the change in intensity at (○) 2.26 and (●) 2.35 Å^{-1} due to the GaN film as a function of thickness. The in-plane epitaxial relationship between GaN and α-Al_2O_3 is $[10\bar{1}0] \parallel [11\bar{2}0]$. The resolution in the $Q_{\|}$ direction is $\approx$0.02 Å^{-1}.

that observed in quasi-layer-by-layer (2D) growth. However, after only one cycle (whose peak occurs at $\approx$1 BL), the oscillations cease and the intensity decays monotonically. The same data are re-plotted versus film thickness instead of time in the inset of Fig. 1b. The specular reflectivity decreases gradually, coming to within 10% of its steady-state value only after the equivalent of 5 BL of GaN have been deposited.

The data in Fig. 1 are consistent with the following model: growth is initiated by the formation of a single GaN BL which grows laterally until it covers a large percentage of the surface. Near the completion of this BL, 3D islands nucleate and grow. The increasing growth rate may be explained qualitatively by the incorporation probability of atoms landing on the first layer being much larger than that of atoms landing on the substrate. The growth rate then increases with coverage. Below, we test this picture quantitatively with a coupled rate-equation growth model (Fig. 1c). First we present observations of GaN strain relaxation behavior during growth.

Figure 2 shows grazing incidence x-ray diffraction measurements monitoring the evolution of the strain of a GaN thin film grown using the same conditions as those used for the film described in Fig. 1. To collect these data, growth was periodically suspended while scans were performed. Before growth (scan labeled 0 BL), there is a peak at $Q_{\|} = 2.35$ Å^{-1} due to the nitridation layer. Since the position of this peak does not correspond to that of any expected surface or bulk phases (indicated in Fig. 2 for reference), we label it as α-$Al_2O_3(0001)$:N. The inset shows the evolution of peak intensities at the positions of the nitridation layer and that of relaxed GaN. As GaN grows, the intensity at the position of the scattering due to the nitridation layer increases, indicating that the GaN is initially *commensurate* with α-Al_2O_3:N. At a thickness of 0.93 BL, scattered intensity begins to appear at the relaxed GaN position. This intensity then increases rapidly while the intensity at the commensurate position begins to saturate. The transition from strained to relaxed growth, which occurs near 0.93 BL, appears to coincide with the transition from smooth to rough growth suggested by the reflectivity and fluorescence data in Figs. 1a and 1b.

Because the structure of the first GaN BL is pseudomorphic with the nitridated sapphire surface, we expect that the details of the α-Al_2O_3:N structure may strongly affect the growth. Although a full characterization of this structure has not yet been performed, we have found that its x-ray diffraction pattern closely resembles that of the well-known $(\sqrt{31} \times \sqrt{31})R \pm 9°$ surface reconstruction of the sapphire (0001) surface. In order to perform this comparison, we prepared the $(\sqrt{31} \times \sqrt{31})$ reconstruction by evaporating Al onto clean sapphire and then heating to 1050 °C following a known procedure [10].

Figure 3a shows a transverse scan passing through the $(6, 4)$ reflections of the $(\sqrt{31} \times \sqrt{31})$ surface reconstruction, which are rotated by $\pm 2.361°$ from the sapphire $[11\bar{2}0]$ axis [11]. It is known that the position of this

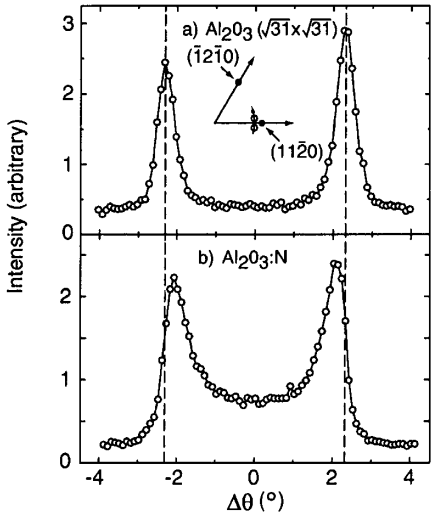

FIG. 3. Grazing incidence azimuthal scans showing the rotated-domain structure of (a) the α-$Al_2O_3(0001)$ $(\sqrt{31} \times \sqrt{31})R \pm 9°$ reconstruction ($Q_\parallel = 2.378$ Å^{-1}) and (b) the α-$Al_2O_3(0001)$:N structure ($Q_\parallel = 2.35$ Å^{-1}). The solid lines are guides to the eye. The dashed lines in the figure and open circles in the inset indicate the ideal locations of the $(6, 4)$ reflections of the $(\sqrt{31} \times \sqrt{31})$ reconstruction, which are $\pm 2.361°$ from the α-Al_2O_3 $[11\bar{2}0]$ direction [11].

peak is determined by the arrangement of 26.5 Å hexagonal domains of Al atoms into a well-ordered 2D lattice. For comparison, Fig. 3b shows a transverse scan through the α-Al_2O_3:N peak position observed in Fig. 2. As in Fig. 3a, most of the intensity is due to reflections that are rotated away from the sapphire $[11\bar{2}0]$ axis. In addition, *in situ* specular reflectivity scans (not shown) suggest that the nitridation layer is approximately 6 Å thick.

Based upon these observations, we propose that the α-Al_2O_3:N structure is a stable surface reconstruction which consists of an array of thin, rotated domains which closely resembles that of the sapphire $(\sqrt{31} \times \sqrt{31})$ reconstruction. The small shift of the peak positions away from commensurate positions (see Figs. 2 and 3) and the additional intensity between the two main peaks (see Fig. 3b) could arise from disorder in the packing of domains between the two structures.

Exposing sapphire (0001) to a nitrogen plasma can also result in the formation of a thin layer of relaxed AlN at the sapphire surface [5,12,13]. We have found that the α-Al_2O_3/AlN structure and the α-Al_2O_3:N surface reconstruction form under nearly identical conditions. This makes it very difficult to prepare one versus the other reproducibly. Heinlein *et al.* [14] find that while a nitridation layer forms on sapphire (0001) in the first few minutes of exposure to nitrogen, exposure times of an hour or more are required for that layer to fully relax to the AlN lattice parameter. Their observation suggests the presence of a surface layer with a smaller lattice parameter than bulk AlN for short exposure times.

The information provided by Figs. 2 and 3 adds substantial insight to the interpretation of Figs. 1a and 1b given above. The first GaN BL, which nearly covers the substrate before subsequent layers nucleate and grow, appears to be pseudomorphic to the α-Al_2O_3:N surface reconstruction, and therefore *strained*. Subsequent growth consists of *relaxed*, 3D islands which nucleate on top of this first BL. As described above, the nonlinearity in the growth rate may be explained as arising from an increase in incorporation probability with increasing GaN coverage. Qualitatively similar effects have been observed for 3D GaN growth [5,7] and for growth of Fe/Si(001) [6]. Quantitatively, however, we find that the nonlinearity reported here is much more pronounced and that existing models [6,7] cannot accurately describe the data.

We model the growing film by a set of coupled differential equations which describe the time evolution of individual layer occupancies θ_i:

$$\frac{d\theta_i}{dt} = S_{i-1}(1 - \alpha_{i-1})(\theta_{i-1} - \theta_i) + S_i\alpha_i(\theta_i - \theta_{i+1}). \tag{1}$$

Following the treatment by Cohen *et al.* [15], α_i is the probability for the interlayer transport of material from layer $(i + 1)$ to layer i. Similar models have been used to model diffraction and STM results obtained for a variety of metal/metal systems [16,17]. In each of these cases, however, the growth rate is constant with respect to time. In our model, a variable growth rate is allowed by the parameters S_i, which represent the incorporation rates onto each layer. Only three independent values of S_i are allowed, representing the incorporation rates on the substrate, on the first layer, and on layers two and higher. Similarly, only α_1 is allowed to be nonzero, while $\alpha_n = 0$ for $n \geq 2$. In other words, interlayer transport is allowed only for adatoms from on top of the first layer to the substrate. Furthermore, α_1 is fixed at unity for occupancies $\theta_1 \leq \theta_C$. This behavior is motivated by the notion of a critical island size as described by Tersoff *et al.* [18]. For occupancies in the range $\theta_C < \theta_1 < 1$, α_1 is assumed to have the following form [15]:

$$\alpha_1 = \frac{d(\theta_1)}{d(\theta_1) + d(\theta_2)}, \qquad d(\theta) = \begin{cases} \sqrt{\theta}, & 0 < \theta < 0.5, \\ \sqrt{1 - \theta}, & 0.5 < \theta < 1. \end{cases} \tag{2}$$

This model allows only downhill transport. If uphill transport occurred, the surface would be expected to continue to roughen if the growth was stopped at an intermediate stage. However, such behavior was not observed.

After numerically integrating Eq. (1), we calculate the film thickness as the sum of individual layer occupancies $\theta_i(t)$. The specular reflectivity at the GaN (0001) is proportional to the square of the scattering amplitude $A(t)$, which is calculated in the kinematic approximation as

$$A(t) \propto A_{\text{sub}}e^{i\phi} + A_{\text{GaN}}\sum_{i\geq 1}\theta_i(t)(-1)^{i-1}. \tag{3}$$

Here, A_{GaN} and A_{sub} are the scattering amplitudes of a single GaN BL and of the substrate, and ϕ is the substrate phase relative to the first GaN BL. The ratio A_{GaN}/A_{sub} and the phase ϕ are very sensitive to unknown details of the α-Al_2O_3:N substrate, and are therefore treated as fit parameters.

The solid lines in Figs. 1a and 1b are the result of a *simultaneous* fit of the fluorescence and reflectivity data to the growth model described by Eqs. (1) and (2). Figure 1c shows the resulting time-dependent layer occupancies $\theta_i(t)$. The best-fit parameters, for which $\chi^2 = 1.2$, are $\theta_C = 0.77 \pm 0.06$, $S_0 = 0.011 \pm 0.002$, $S_1 = 0.35 \pm 0.02$, $S_{n>1} = 1.75 \pm 0.07$, $A_{GaN}/A_{sub} = 1.95 \pm 0.06$, and $\phi = 2.46 \pm 0.02$ radians.

The quality of the fit supports the interpretation of Figs. 1a and 1b given above. The increasing growth rate arises from the large increase in incorporation probability ($S_{n>1} \gg S_1 \gg S_0$). The highly nonlinear nature of this increase, however, involves both this increase and the high probability of interlayer transport ($\alpha_1 = 1$) for $\theta_1 < \theta_C$. The rate equation for the first layer at small occupancies then becomes $d\theta_1/dt \approx S_1\theta_1$, leading to an exponential form. Physically, this corresponds to a propensity of adatoms landing on top of 1 ML islands to hop down to the substrate and attach at island edges, so that an island's growth rate is proportional to its size. Thus the nonlinearity in growth rate results from a combination of the incorporation probability, which is less than one because of desorption of Ga and N precursors, and the interlayer transport probability, which controls the film morphology.

We have previously found that ion-assisted GaN growth using ionized NH_3 on α-Al_2O_3/AlN occurs in an extended layer-by-layer mode [5] rather than the 2D-to-3D mode observed here. This suggests that an AlN nitridation layer could be more favorable for promoting a 2D growth mode than the α-Al_2O_3:N surface. Both types of nitridation layer are much more closely lattice matched to GaN than sapphire, and therefore effectively reduce the 16% sapphire/GaN lattice mismatch. However, between these two structures (see Fig. 2), AlN is more closely lattice matched to GaN than α-Al_2O_3:N.

The 2D-to-3D growth mode observed here does not necessarily represent the true equilibrium structure, as in the case of Stranski-Krastanow growth [19]. Our rate-equation model explains the observed transition as due primarily to abrupt changes in incorporation probability and interlayer transport probability, i.e., a purely kinetic effect. The surface of the growing film therefore may not assume the lowest energy structure. However, there is a clear link between structure and growth mode, which manifests itself in the model as an abrupt change in both the incorporation and interlayer transport parameters in coincidence with strain relaxation.

In conclusion, we have shown that incorporation and interlayer transport are intimately linked to surface structure and strain relaxation during kinetically limited gas source growth. Detailed understanding of the substrate surface and incorporation kinetics is therefore invaluable in controlling the nucleation and growth, and ultimately the structure and properties of thin GaN films.

We thank Jim Sethna for many helpful discussions and M. V. Ramana Murty for technical assistance. This research program is supported by the Cornell Center for Materials Research (CCMR) which is supported by the National Science Foundation (NSF) through Grant No. DMR-96-32275. CHESS is supported by the NSF through Grant No. DMR-97-13424.

[1] Z. Zhang and M. G. Lagally, Science **276**, 377 (1997), and references therein.
[2] C. W. Snyder, B. G. Orr, D. Kessler, and L. M. Sander, Phys. Rev. Lett. **66**, 3032 (1991).
[3] J. Tersoff, C. Teichert, and M. G. Lagally, Phys. Rev. Lett. **76**, 1675 (1996).
[4] R. L. Headrick *et al.*, Phys. Rev. Lett. **65**, 1128 (1990).
[5] R. L. Headrick *et al.*, Phys. Rev. B **58**, 4818 (1998).
[6] B. K. Kellerman *et al.*, Surf. Sci. **375**, 331 (1997).
[7] R. L. Headrick *et al.*, Phys. Rev. B **54**, 14 686 (1996).
[8] The fluorescence is calibrated by *ex situ* measurements of film thickness using Rutherford backscattering spectrometry.
[9] The growth conditions used here were chosen to be in a Ga-limited regime on the basis of *ex situ* characterization of large number of calibration samples. Post-growth AFM measurements show no evidence of Ga droplet formation.
[10] T. M. French and G. A. Somorjai, J. Phys. Chem. **74**, 2489 (1970).
[11] G. Renaud, B. Villette, I. Vilfan, and A. Bourret, Phys. Rev. Lett. **73**, 1825 (1994).
[12] M. Yeadon *et al.*, J. Appl. Phys. **83**, 2847 (1998).
[13] N. Grandjean, J. Massies, and M. Leroux, Appl. Phys. Lett. **69**, 2071 (1996).
[14] C. Heinlein *et al.*, J. Appl. Phys. **83**, 6023 (1998).
[15] P. I. Cohen *et al.*, Surf. Sci. **216**, 222 (1989).
[16] H. A. van der Vegt *et al.*, Phys. Rev. Lett. **68**, 3335 (1992).
[17] H. Röder, K. Bromann, H. Brune, and K. Kern, Surf. Sci. **376**, 13 (1997).
[18] J. Tersoff, A. W. Denier van der Gon, and R. M. Tromp, Phys. Rev. Lett. **72**, 266 (1994).
[19] I. N. Stranski and L. Krastanow, Sitz. Ber. Akad. Wiss. Wein. **146**, 797 (1938).